ORIGINAL ARTICLE

lajss.org© Latin American Journal of Solids and Structures

www.lajss.org

Dynamic Response Analysis of Geogrid Reinforced Embankment Supported by CFG Pile Structure During a High-Speed Train Operation

Ishola Valere Loic Chango[a]

Muhan Yan[a]*

Xianzhang Ling [a, c]

Tang Liang[a]

Ogoubi Cyriaque Assogba[b]

[a] School of Civil Engineering, Harbin Institute of Technology, Harbin 150090, China, E-mail: chanshola@gmail.com; chanshola@hit.edu.cn, ymh_hit@163.com, lxz_hit@163.com, hit_tl@163.com

[b] School of Transportation Science and Engineering, Harbin Institute of Technology, Harbin 150090, China, assocyr@hotmail.fr, assocyr@stu.hit.edu.cn,

[c] School of Civil Engineering, Qingdao University of Technology, Qingdao, Shandong 266033, China.

* Corresponding author

https://doi.org/10.1590/1679-78255710

Abstract

The performance of railroad structure has a tremendous influence on the safety and stable operation of high-speed trains. Strong vibrations and the degradation rate of the track are the main factors affecting the transport safety of a railroad built over a weak soil. Geogrid reinforced embankment supported by pile structure is a new efficient construction technique used to ensure the stability and enhance the performance of the railroad system; but only a few studies are oriented to its behavior under train operation. This paper investigates the dynamic response of geogrid reinforced embankment supported by cement fly-ash gravel pile structure during a high-speed train operation. The establishment of a realistic simulation model for railroad subjected to a moving train load, is an important first step towards the reliable design of geogrid reinforced embankment supported by pile structure. Thus, a 3D nonlinear FEM has been established to simulate the instrumented Harbin-Dalian railway test section. Each train carriage was modeled as a transient dynamic load through a user-defined Dload subroutine. The developed model was successfully validated by the dynamic response recorded from the field test section. The improvement of the railroad structure by the CFG piles and geogrids contributed significantly to the reduction of the vibration in the structure, which attenuates 1.2 times faster with the structure depth, even under overload conditions. Moreover, the phenomenon of resonance observed when the train reaches speeds of 100 and 260 km/h were annihilated. The analysis of the stress distribution within the embankment revealed that a dynamic arch is formed in the embankment at 2 m from the ground. The stress onto the pile was 16 times greater than that acted on the soil and the tensile stress developed in the geogrid was high at the piles edge below. In addition, the coupling effect of geogrid with various tensile strengths and the piles with different strength grades indicated that the combination of a high-strength pile and geogrid significantly reduces the displacement gap due to the variation of train speed. As a result, the vibrations of the track were almost constant during the train operation; thus, ensuring comfort to passengers and reducing the risk of derailment.

Keywords

dynamic response; 3D-FEM; transient dynamic train load; pile; geogrid, vibration.

Received: June 28, 2019. In Revised Form: July 08, 2019. Accepted: July 11, 2019. Available online: July 15, 2019.
http://dx.doi.org/10.1590/1679-78255710

Latin American Journal of Solids and Structures. ISSN 1679-7825. Copyright © 2019. This is an Open Access article distributed under the terms of the Creative Commons Attribution License, which permits unrestricted use, distribution, and reproduction in any medium, provided the original work is properly cited.

1 INTRODUCTION

The development of the high-speed railroad in recent years has improved the transportation system around the world and has contributed immensely to countries' economies. However, the railway construction on low bearing soil remains a major challenge for engineers who must ensure the structure stability by minimizing various deformations and vibrations. It is known that the high-speed train movement along the railway generates dynamic forces and vibrations. Several studies have been done to investigate the dynamic behavior of railroad and the effect of weak soil on train safety were pointed out, which describes the risk of train derailment due to significant dynamic amplifications that take place in the structure as a certain critical speed is approached by the train[1-4].

The ground enhancement with pile and geogrid reinforced embankment is widely used, as an effective, economical and fast technique for highway and railroad constructions in solving the problems associated with the low bearing capacity of the soil [5]. Many investigations have shown that such a structure provides better stability and the various settlements were reduced [6, 7]. Other studies have focused on the distribution of loads in the structure as well as new methods for analysis and design to improve its performance [8-12]. Since these structures were built to accommodate rolling loads, most of the research has been carried out under static load. Little is known of its dynamic behavior under a moving train load. Most research problems till now, have been solved mathematically or by assumption in view of the results obtained from studies carried out under embankment load.

The use of auxiliary rails reduced the rail variation deflection along the transition zone [13]. Real investigated the influence of the railway component on the vibration behavior of the track and found that the vibration in the concrete sleeper is lower than the one in the wood sleeper [14]. Sol-Sánchez found that the use of deconstructed end-of-life tires in the manufacture of rail pads improves the performance of rail tracks [15]. Even though these previous works dealt with the the performance of the railroad, the dynamic response enhancement of the. Railway system can not be limited only to track components. In some cases, the damages may be more severe due to the low bearing capacity of the ground and the low rigidity of the embankment. The dynamic response of the geogrid reinforced embankment supported by pile structure during the passage of the train is a very complex phenomenon. It is unfortunate, however, that very few experimental and numerical studies have given a comprehensible explanation on it. It is, therefore, necessary to study the characteristics of an existing railway embankment reinforced by a geogrid and supported by a CFG pile using a numerical model. Compared to ordinary heavy haul train, the high-speed train cause more structural vibration to the railroad during its operation. Moreover, the dynamic response characteristics of a geogrid reinforced high-speed railroad embankment supported by CFG pile are very different from those of a railroad embankment supported only by piles. Therefore, it is necessary to explore the dynamic characteristics of the geogrid reinforced railroad embankment supported by CFG pile and to better elucidate the mechanism of the system components interaction, which is of great importance to the establishment of stringent guidance for the railroad design over weak soil.

In this study, a 3D finite element model was implemented in Abaqus with the dynamic train load performed as a transient local dynamic load by using a subroutine Fortran. The concrete damage plasticity behavior was included in the properties of the pile for more accurate characterization of its behavior. By comparing the computed results with the dynamic stress and accelerations obtained from field measurements of the Harbin-Dalian high-speed railroad in China, the numerical model reliability for the analysis of the railroad dynamic response has been checked. After that, the influence of the CFG pile and the geogrid on the railroad system vibration was evaluated. The distribution of the stresses within the geogrid reinforced railroad embankment supported by CFG pile structure was also investigated. Finally, the coupling effect of pile and geogrid with various strength on the vibration variation along the track due to the speed change of the train during the operation were also analyzed.

2 Numerical Modelling of Geogrid Reinforced and Pile Supported Embankment Railway

This section includes the description of a three-dimensional model of the railroad embankment reinforced by geogrid and supported by pile, the material parameters, the dynamic train load model, the mesh and boundaries conditions.

2.1 Model Geometry

The three-dimensional FEM model developed, was based on the Harbin-Dalian railway section constructed in 2010. The railroad bed surface width is 13.6 m and the height is 5.433 m with a slope ratio of 1:1.5. As depicted in Figure 1, the railroad bed upper layer is the well-graded gravel of 0.40 m. The layer localized below the graded gravel is non-frost heaving group filling A/B. The following respective layers are; the normal A/B group fill, normal A/B/C group fill and a cushion layer in which two geogrid layers are embedded. The foundation soil, composed of a loess clay of 10 m, a silty

clay layer of 10 m and the silt layer of 12 m, is reinforced by the cement fly-ash gravel piles (CFG-piles) of 20 m of length and 0.5 m of diameter with a strength of C25. The piles' layout is an equilateral triangle of 1.5 m spacing [16, 17]. The embankment surface is covered by CRTS (China Rail Track System) type-I which include the rail, fastener system, track slab, CA mortar, resin material and concrete roadbed [18].

Considering the advantage of symmetry, the geometry section was made simpler to one half in the FEM built in Abaqus 6.14 as depicted in Figure 2. Its total length is 120 m and a width of 25 m. The Euler Bernoulli beam element has been adopted to model the rail. A tie connection was utilized to ensure mutual contact between the layers under the track slab with the continuity of the interface's deformation and the geogrid was embedded in the cushion layer [19, 20]. A system of Cartesian coordinate was adopted in which the railroad transverse direction is indicated by the X-axis, the vertically downwards is the Y-axis and longitudinal direction (train moving direction) is indicated by the Z-axis.

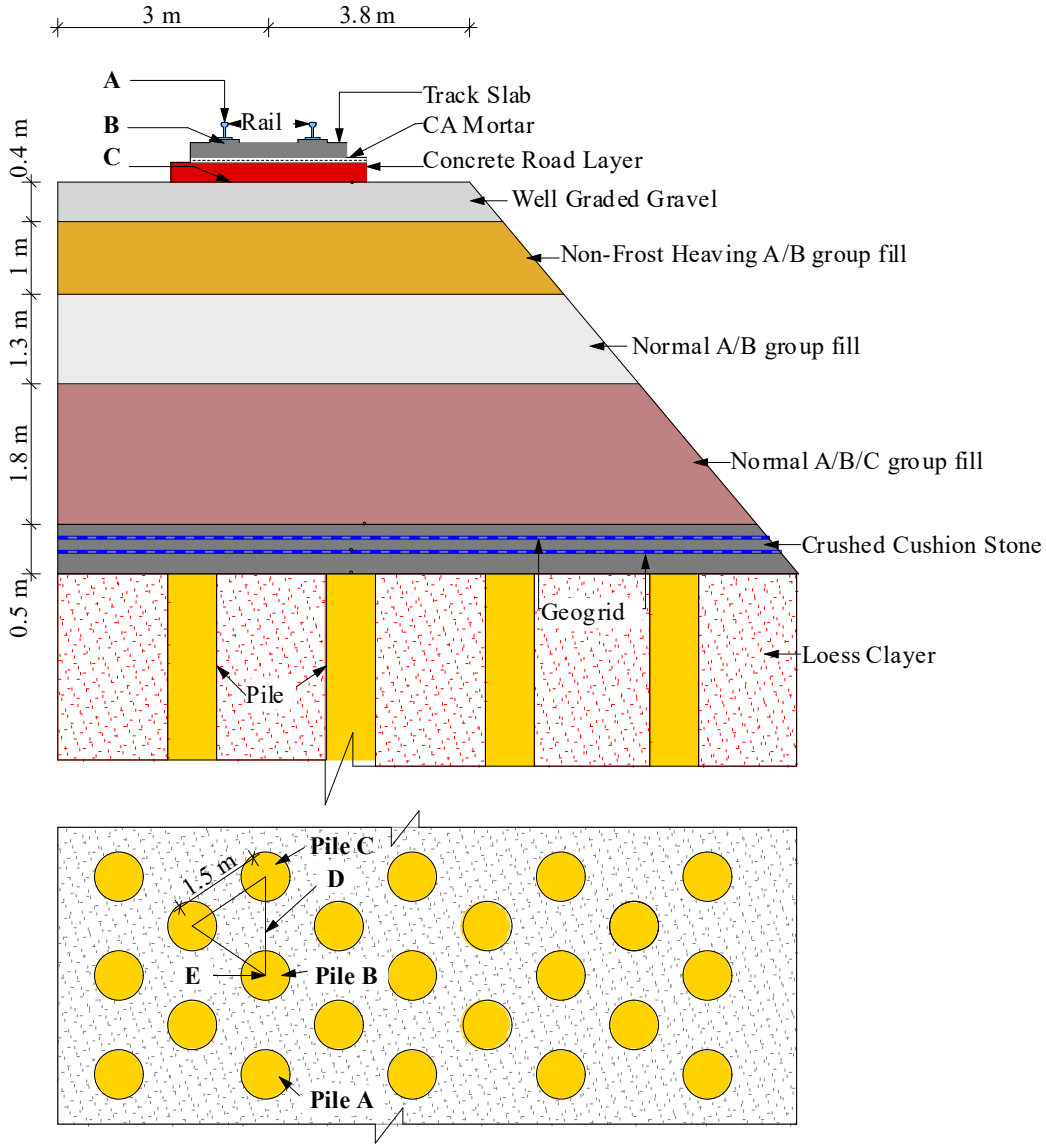

Figure 1 The geometry of Railway passenger Harbin-Dalian Study

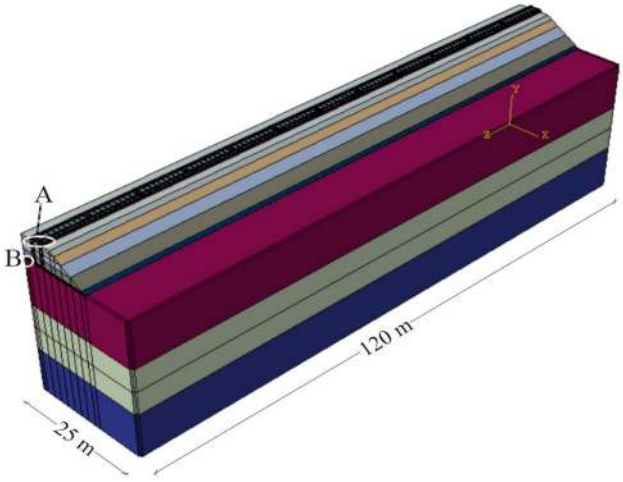

a) View of 3-D railway model

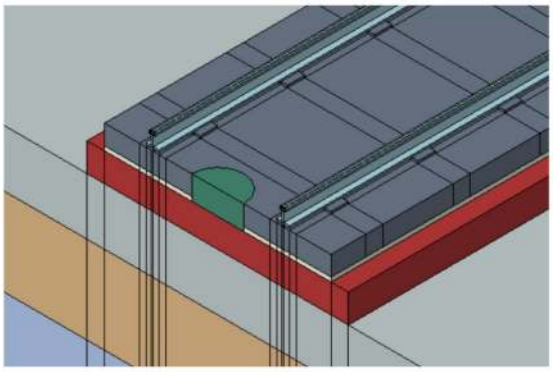

b) View A of Railway track

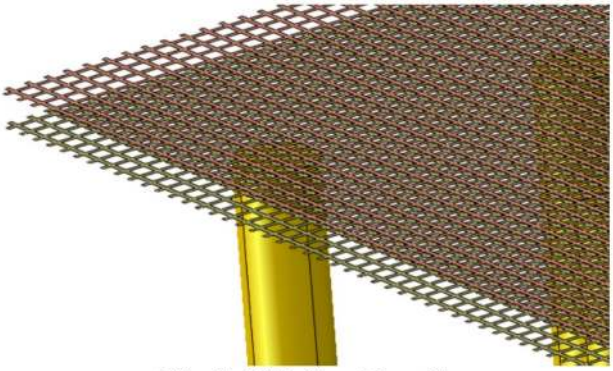

c) View B of CFG pile and Geogrid

Figure 2 Three-dimensional railway model

2.2 Material Characterization

The properties of materials and specification values were based on previous works [17, 18]. Founded on elastic layered system hypothesis, railroad track and embankment materials are all linear elastic. The rail-base rubber pads and the fasteners between track slab and rail are taken on as linear elastic components and have been modeled using spring-damper elements with a stiffness value of 45 kN/mm and the coefficient of damping is 45 kN s/m [21]. The soil layers are supposed to be elasto-plastic by using the Mohr coulomb model [19]. The interaction between the materials is supposed to be completely continuous. The equivalent parameters are recapitulated in Table 1. The piles are elasto-plastic by using Concrete Damage Plasticity The stress plastic strain relation of concrete and damage –strain relation at different grades: C25, C60, and C80 were presented in Table 2, Table 3 and Table 4. Geogrids were modeled as an isotropic linear elastic membrane with an ultimate tensile strength of 30 kN/m and a Poisson ratio of 0.3.

Table 1 Materials properties

Material	Elastic Modulus (MPa)	Density (Kg/m^3)	Poisson Ratio	Cohesion (kPa)	Friction angle (°)
Rail	210000	7800	0.3	-	-
Track Slab	39000	2500	0.3	-	-
CA Mortar	100	1800	0.3	-	-
Concrete Base	32500	2500	0.27	-	-
Graded Gravel (Roadbed)	310	1800	0.3	-	-
Non-frost Heaving Group Filling A/B	298	2060	0.3	-	-
Group Filling A/B	350	2080	0.3	-	-
Group Filling A/B/C	298	1980	0.3	-	-
Cushion Crushed Stone	300	1850	0.3	-	-
Clay Loess	19	1850	0.35	13	12
Silty Clay	19	1650	0.4	11	9
Silt	27	1880	0.35	17	19

Table 2 CFG Pile with strength grade C25

Elasticity Modulus (MPa)	Poisson ratio	Dilatation angle	Eccentricity	Stress ratio σ_{bo}/σ_{co}	Pressure ratio Kc	Viscosity parameter	
28000	**0.2**	**30**	**0.1**	**1.16**	**0.667**	**0.0005**	
Compression hardening		Tension stiffening		Compression Damage		Tension damage	
Stress (kN/m^2)	Strain x10^{-3}	Stress (kN/m^2)	Strain x10^{-3}	Damage d_c	Strain x10^{-3}	Damage d_t	Strain x10^{-3}
11690	0.000	1797.8	0.000	0.000	0.000	0.000	0.000
16700	0.809	1780	0.0260	0.010	0.809	0.010	0.026
13239.8	2.34	1191.06	0.136	0.207199	2.34	0.330864	0.136
9841.27	3.86	859.483	0.236	0.410702	3.86	0.517144	0.236
7674.36	5.35	684.527	0.332	0.540458	5.35	0.615434	0.332
6248.49	6.80	576.455	0.425	0.69718	6.80	0.747045	0.425
5255.01	8.24	502.469	0.516	0.78611	8.24	0.834016	0.516
4527.98	9.67	448.233	0.608	0.84114	9.67	0.888637	0.608
3974.73	11.1	406.519	0.698	0.877465	11.1	0.919064	0.698
3540.4	12.5	373.278	0.789	0.902661	12.5	0.937999	0.788
		131.57	3.800			0.998225	3.560

Table 3: CFG Pile with strength grade C60

Elasticity Modulus (MPa)	Poisson ratio	Dilatation angle	Eccentricity	Stress ratio σ_{bo}/σ_{co}	Pressure ratio Kc	Viscosity parameter	
36000	**0.22**	**30**	**0.1**	**1.16**	**0.667**	**0.0005**	
Compression hardening		Tension stiffening		Compression Damage		Tension damage	
Stress (kN/m^2)	Strain x10^{-3}	Stress (kN/m^2)	Strain x10^{-3}	Damage d_c	Strain x10^{-3}	Damage d_t	Strain x10^{-3}
26950	0	2878.50	0.000	0.000	0.000	0.0000	0.000
38500	0.701	2850.00	0.036	0.010	0.700	0.0100	0.036
19978.3	0.298	1256.67	0.195	0.481084	2.980	0.559063	0.195
11087.9	5.00	760.756	0.323	0.712003	5.00	0.733068	0.323
7444.03	6.87	558.434	0.444	0.806648	6.87	0.804058	0.444
5552.82	8.70	448.564	0.562	0.876252	8.7	0.877995	0.562
4412.21	10.0	379.016	0.678	0.913899	10.5	0.922909	0.678
3654.2	12.3	330.681	0.794	0.936577	12.3	0.949666	0.794
3115.66	14.1	294.926	0.910	0.951309	14.1	0.964133	0.910
2714.07	15.9	267.272	1.06	0.961426	15.8	0.972937	1.03
		86.0337	4.59			0.999299	4.59

Table 4: CFG Pile with strength grade C80

Elasticity Modulus (MPa)	Poisson ratio	Dilatation angle	Eccentricity	Stress ratio σ_{bo}/σ_{co}	Pressure ratio Kc	Viscosity parameter	
38000	**0.22**	**30**	**0.1**	**1.16**	**0.667**	**0.0005**	
Compression hardening		Tension stiffening		Compression Damage		Tension damage	
Stress (kN/m^2)	Strain x10^{-3}	Stress (kN/m^2)	Strain x10^{-3}	Damage d_c	Strain x10^{-3}	Damage d_t	Strain x10^{-3}
35140	0	3141.1	0.000	0.000	0.000	0.000	0.000
50200	0.038	3110	0.037	0.01	0.601	0.01	0.039
22358.2	0.208	1239.38	0.202	0.554618	3.26	0.601485	0.208
11618.5	5.46	728.476	0.342	0.768556	5.46	0.765763	0.342
7601.82	7.49	528.471	0.467	0.848569	7.49	0.830074	0.467
5596.63	9.46	421.811	0.59	0.902677	9.47	0.895181	0.59
4412.34	11.4	354.989	0.712	0.931921	11.4	0.934206	0.712
3635.46	13.4	308.862	0.834	0.94959	13.4	0.957244	0.834
3088.38	15.3	274.904	0.95	0.961115	15.3	0.969631	0.955
2683	17.2	248.735	1.08	0.969065	17.2	0.977139	1.08
		79.2484	4.81			0.999416	4.81

2.3 Mesh and Boundaries Conditions

In order to accurately simulate railroad dynamic response, various mesh sizes were chosen to respect the convergence of calculations and optimal sizes of elements by referring to [22]. In this study, the fine mesh was utilized in the area below the application path of the train carriages where stress and displacement are high. A dense size mesh was adopted near the load application zone and the relatively coarse mesh was used far away from the load application zone.

The mesh of geogrid is defined as an M3D4R (4-node quadrilateral membrane with reduced integration and hourglass control). An 8-node linear brick with reduced integration and hourglass control (C3D8R) was utilized for the track slab, the CA Mortar layer, the concrete base, the subgrade, the soil and pile [23]. The boundaries conditions have a great influence on the numerical model computation of dynamics problems. The most used methods are infinite element boundaries and traditional boundaries. The infinite boundaries conditions reduce the wave reflection effect and absorb stress wave at the boundary surface. All in all, the infinite boundary gives a more precise result compared to conventional boundaries. In this study, the symmetry boundary is restrained from the translation in the x-direction due to symmetry advantage considered by halving the geometry section.

As it is depicted in Figure 3, a 3-D continuum solid of infinite elements with 8-node linear (CIN3D8) were utilized on the remains faces to describe the infinite boundary condition [24, 25]. The three-dimensional model is composed of 5042302 finite and infinite elements and 9430974 degrees of freedom.

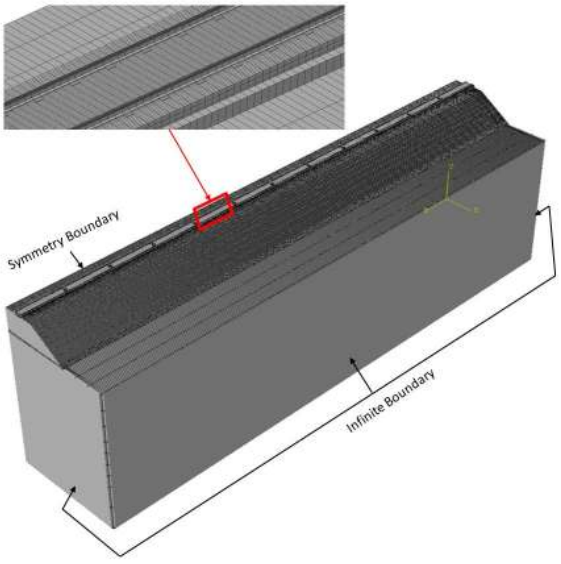

Figure 3 Mesh of the finite element model

2.4 Dynamic Train Moving Load

The high-speed train load moving along a rail is a combination of incessantly dynamic load changes and static load. In reason of train reaction on the longitudinal unevenness of the rails, the dynamic load causes a local augmentation of the total load. Railway track profile, train speed, carriages mass, and train suspension system are the main factors which affect the dynamic part of the total load. The dynamic train load is simplified by the continuous change of the loading amplitude.

The basic motion equation can be resolved by an implicit process because of its effectiveness for a structural dynamic problem such as in [26, 27].

$$[M]\{\ddot{U}\}+[C]\{\dot{U}\}+[K]\{U\}=\{P\} \tag{1}$$

Where, [M] represents mass matrix [C] represents damping matrix; [K] represents stiffness matrix; {P} is the external force vector; $\{\ddot{U}\}$ is an acceleration vector $\{\dot{U}\}$ represents velocity vector and $\{U\}$ represents displacement vector.

The high speed train used was based on a CRH3 vehicle model, frequently used in China. It consisted of eight cars of 25 m each as depicted in Figure 4. The wheels, axles, and body of the train carriage were considered like rigid parts with the connections represented as spring-damper elements. It has been assumed that each car is perfectly symmetrical and can be divided into 4 parts. Each axle is associated with the bogie via a primary suspension; the bogie is associated with the body of the carriage via a secondary suspension. In this study, only vertical carriage and rail movements were taken into account. Moreover, it is assumed that the rail and the wheel do not separate during the operation. This means that there is no relative vertical displacement. The dynamic train load was performed as a transient local dynamic load by using a subroutine to specify the non-uniform distributed load (DLOAD), which allows users to specify the distributed load magnitude variation as a time function (TIME*), coordinate (COORDS*), domain element number and applied load integration point number [28]. The train moving load effect, developed in Fortran and incorporated into the implicit dynamic analysis, was based on wheel-rail contact force equation [29]. The wheel-rail contact force of the ith wheel in the nth carriage was described as follows:

$$P_{ni}\left(x-vt\right)=P_{ni}\delta\left(x-vt++2a_n+b_n+\sum_{s=0}^{n-1}L_s+L_0\right) \tag{2}$$

Where x is the distance between the axle of the train and a reference point in front of the train; v is the train speed; t is the time; L_0 is the distance between the head of the train and a reference point in the running direction of the train; L_s is the (n-1) length of a carriage; a_n is the distance of two-wheel axle in the nth carriage; b_n is the distance between two adjacent axles in two bogies of the nth car.

The computation parameters of Equivalent Force of the high speed train was recapitulated in Table 5.

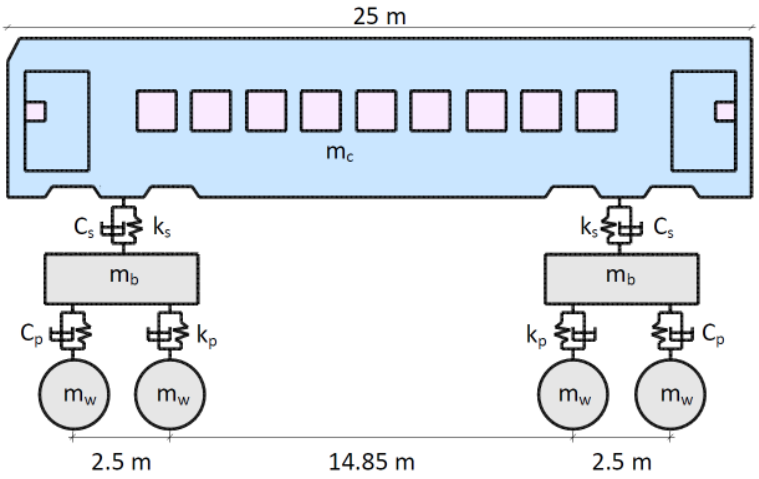

Figure 4 Carriage train Geometry

Table 5: Parameters for Computation of Equivalent Forces

Mass of carriage (kg)	40000	Length of a Carriage (m)	25
Mass of Bogie (kg)	3200	Stiffness of primary suspension spring (N/m)	2080000
Mass of Wheel Axle (kg)	2400	Damping of primary suspension spring	100000
Axle Load (kN)	140	Stiffness of secondary suspension spring (N/m)	800000
Distance of Wheel Axle in a Bogie (m)	2.50	Damping of primary suspension spring	120000
Distance of Bogies in a Carriage (m)	14.85		

2.4 Material Damping

The damping of material is a factor that affects a structure dynamic response. In finite element analysis, it is not simple to determine accurately the matrix of damping because of its complexity. In general, the damping calculation methods used are modal damping method, stress energy factor method, Rayleigh damping method, and stiffness factor method. For the structural dynamic analysis, Rayleigh Damping is generally used and expressed in Eq. (3).

$$C = \alpha M + \beta K \tag{3}$$

Where [C] represents damping matrix of the physical system; [M] represents mass matrix of the physical system; [K] represents the system stiffness matrix; α and β are the predefined constants.

Damping coefficient α and β depend on the structure natural frequency of and the damping ratio.

$$\alpha = \frac{2\omega_1\omega_2}{\omega_1 + \omega_2}\xi_0 \tag{4}$$

$$\beta = \frac{2}{\omega_1 + \omega_2}\xi_0 \tag{5}$$

where, ξ_0 represents damping ratio.

In order to define the Rayleigh damping, a finite element modal analysis was performed. Extraction of the first 50 natural circular frequencies was done to fix the essential frequency ω1 and selected ω2 among higher order vibration modes. Therefore, ω_1 and ω_2 are 16.26 rad/s and 18.91 rad/s respectively. The damping ratio is selected within a span of 2-4% [22]. From these values defined above, the mass proportional damping constant α and stiffness proportional damping constant β computed are 0.5269 and 0.0017 respectively.

3 Model Validation with Field Measurement

3.1 Rail Track Section Instrumentation and Field Testing

The section tested was the Harbin-Dalian high-speed railway with double line track slab China railway system. In order to get the vibration induced by the movement of the high-speed train on the structure, a field test was carried out to measure the acceleration and the dynamic stress. The dynamic stress sensors components were mounted at the external flank of the rail. Some accelerometers were mounted at the track slab surface and others were mounted at the embankment shoulder near the concrete base and facing the rail fulcrum as depicted in Figure 5. The sensor of dynamic stress was DH1205 78 mm gauge length with a resistance of 350 Ω; a range of operating temperature from -20 to +80 °C and designed by Jiangsu Donghua Testing Technology Co. Ltd. The accelerometer sensors were TG-1 model designed by Beijing Taize Technology Development co. LTD, with a frequency range from 0 Hz to 3000 Hz, measurable acceleration field ranging from 0. 1 to 10 g; a linearity of 3% F.S, the sensitivity, a sensitivity of 1-2% F.S, a working power from 5VDC to 24VDC, an output voltage range from 0.5V to 4.5V and an operating temperature varying from -40°C to 105°C

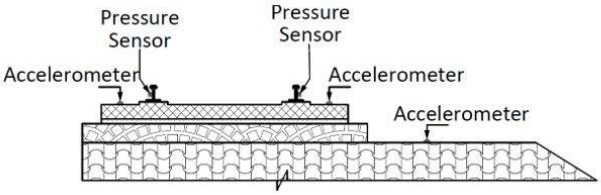

(a) Layout of sensors



(b) Emplacement of sensors



(c) Overview of the test section



d) Data acquisition system

Figure 5: Harbin-Dalin railway test section

3.2 Comparative Analysis between FE Result and Field Measured Data

In this section, the results computed with the numerical model have been compared with the data recorded from the field test to further validate the reliability of the transient local dynamic train load using a Fortran subroutine and the Three-Dimensional Finite Element Model implemented in Abaqus. While the test train was operating at 200 km/h, dynamic stress and vibration acceleration were measured by the various sensors in real time. Based on the geometric parameters of the cross section of the high-speed railroad (Harbin-Dalian section), a three-dimensional numerical model has been established. Figure 6, 7 and 8 compare the dynamic stress and vibration acceleration of the typical locations obtained from the numerical simulation with the field measurement data at the train speed of 200 km/h.

Figure 6 shows the dynamic stress exerted on the rail flank resulting from the field experiments and the dynamic stress exerted on the rail flank resulting from the simulation. There is a strong correlation between the measured dynamic stress of the field and that of the simulation. The peak of the dynamic stress corresponding to the passage of each wheel is visible and similar with respect to timing, shape, and magnitude. The obtained maximum dynamic stress from the field test and simulation were respectively 10.20×10^3 kPa and 9.76×10^3 kPa. The numerical model predicts the contact train wheel rail force successfully with a difference of 4.32%.

Figure 7 shows the vibration acceleration at the track slab from the field measurement and the simulation results. The time histories of the vibration acceleration contain a series of periodic wave shapes and each wave shape cycle corresponds to two bogies of the train. These are the bogies in the back of a carriage and the one at the head of the next carriage. A strong correlation exists between the vibration acceleration from the field measurement and that from the simulation results. The maximum acceleration obtained from field measurement and numerical simulation were 1.1 m/s^2 and 1.04 m/s^2 respectively. The reported difference is 5.45%.

Figure 8 shows the vibration acceleration at the embankment top from the field measurement and the simulation results. The time histories of the vibration acceleration contain a series of periodic wave shapes and each wave shape cycle corresponds to two bogies of the train. these are the bogies in the back of a carriage and the one at the head of the next carriage. A strong correlation exists between the vibration acceleration from the field measurement and that from

the simulation results. The maximum acceleration obtained from field measurement and numerical simulation were 0.93 m/s2 and 1.01 m/s^2 respectively. In this case, the reported difference is 7.92%. These differences may be due to the aliases climatic. A favorable agreement was obtained between the field test and simulation results by considering all the factors cited above. Therefore, the use of a 3D finite element model, for dynamic response prediction of railroad subjected to transient dynamic train load, is appropriate.

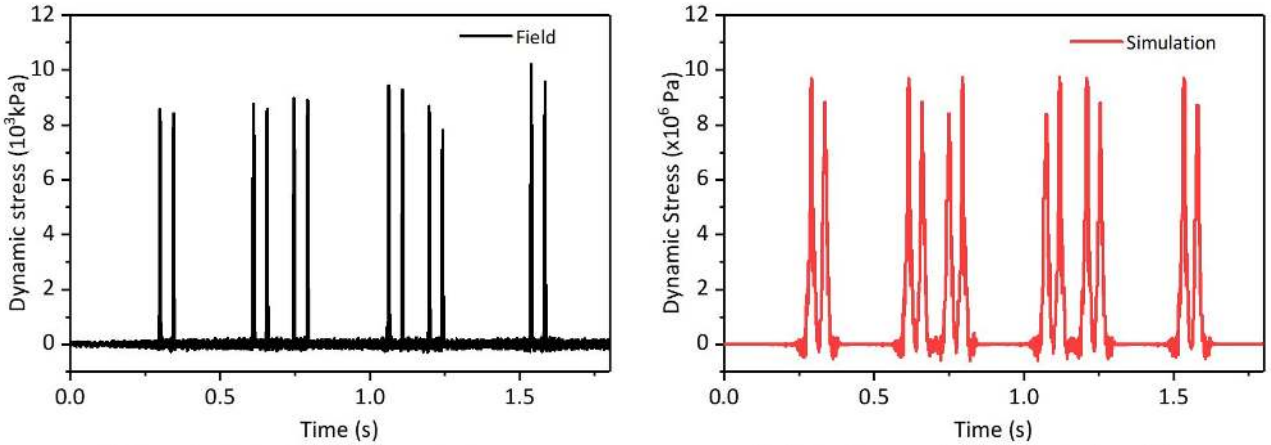

a) Dynamic stress from field meaurement *b) dynamic stress from numerical model*

Figure 6 Dynamic stress at the rail flank at train speed of 200 km/h

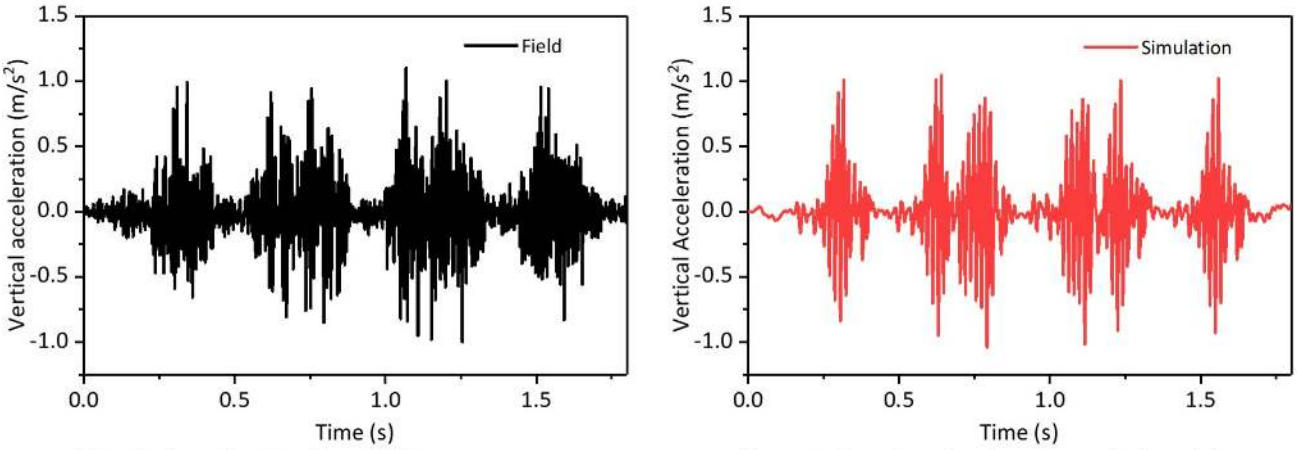

a) Vertical acceleration from field measurement *b) vertical acceleration from numerical model*

Figure 7 Vertical acceleration at the track slab Up at train speed of 200 km/h

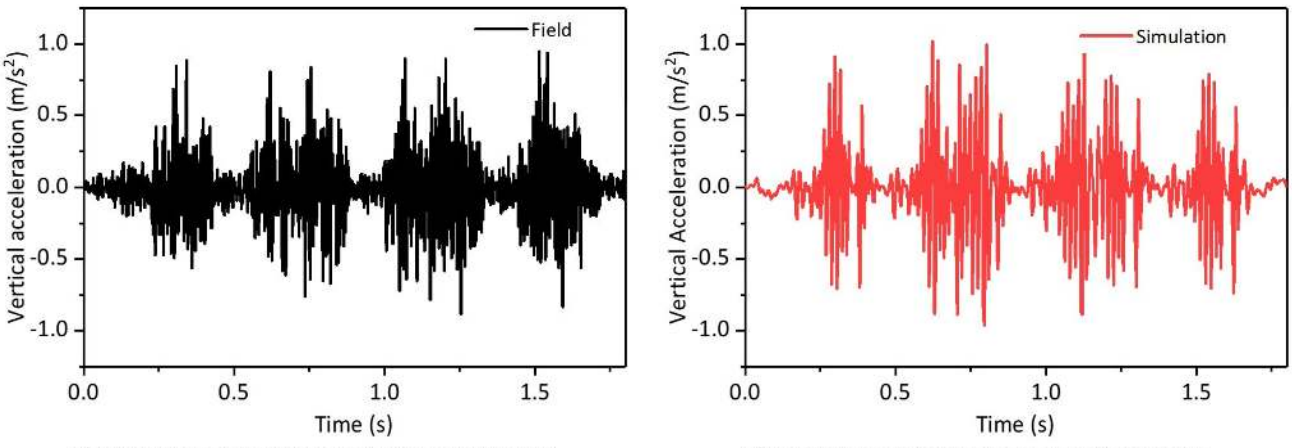

a) Vertical acceleration from field measurement *b) vertical acceleration from numerical model*

Figure 8 Vertical acceleration at the embankment up at train speed of 200 km/h

4 Dynamic Response Analysis of Geogrid Reinforced Railroad Embankment Supported by CFG Pile System

In order to investigate the performance of geogrid reinforced embankment supported by pile structure, the evaluation effect of pile and geogrid on the dynamic response of railroad; the effect of speed and load; the stress distribution and the influence of the reinforcements' strength on the attenuation of vibration due to variation of train speed were analyzed.

4.1 Evaluation Effect of Pile and Geogrid in the Railroad System Subjected to Train Load Moving

To evaluate the role of the pile and geogrid in a railroad dynamic response built over weak soil, the geogrid reinforced embankment supported by CFG pile structure condition was compared to the case of the conventional embankment (structure without pile and geogrid) when the train speed was 200 km/h

4.1.1 Vertical Displacement

The coupling effect of the pile and the geogrid on the vibrations of the railroad structure over weak soil at various locations has been studied. The time histories curves of the vertical displacement at point A, point B, point C, and point D, are illustrated in Figure 9. The position of each wheel can easily be identified at point A.

The vertical displacement for the case of geogrid reinforced embankment supported by CFG pile is less than the conventional embankment at all calculation point. Similarly, there is a significant difference between the maximum displacements of the two cases. At point A, the peak displacement for the geogrid reinforced embankment supported by CFG pile being 39.77% lesser; at point B, the peak displacement for the geogrid reinforced embankment supported by CFG pile being 46.47% lesser; at point C, the peak displacement for the geogrid reinforced embankment supported by CFG pile being 46.66% lesser; and at point D, the peak displacement for the geogrid reinforced embankment supported by CFG pile being 58.01% lesser, as summarized in table 6. These observations can be explained as follows: firstly, the insertion of the pile into the soil improves the bearing capacity of the clay layer whose weakness is the main cause of the great displacement observed in conventional embankments. Secondly, the geogrids reinforce the embankment, which offers greater compressive strength. Thus, the dynamic load effect is reduced on the railroad structure. Moreover, the rate of vibration reduction varies from one typical point to another. This phenomenon can be interpreted by the ability of each material to deform less when subjected to a load. Thus, the coupling effect of the pile and the geogrid depends on the stiffness of each material in the structure and therefore more significant when the material is softer.

In addition, to better understand the role of the pile and geogrid in the vibration attenuation with the structure depth, an attenuation coefficient is defined as:

$$k = \frac{U_x}{U_0} \tag{6}$$

Where U_o is the maximum value of the vertical displacement at point A (rail top) and U_x is the maximum value of the vertical displacement at another point (B, C or D). For the geogrid reinforced embankment supported by CFG pile structure, the attenuation coefficient is 0.818, 0.805, and 0.61 at point B, point C, and point D respectively. For the conventional embankment structure, the attenuation coefficient is 0.913, 0.909 and 0.875 at point B, point C, and point D respectively. For the geogrid reinforced embankment supported by pile structure, at point B, the vibration is about 81.8% of the vibration at point A; at point C, the vibration is about 80.5% of the vibration at point A; at point D, the vibration is about 61% of the vibration at point A. For the conventional embankment structure, at point B, the vibration is about 91.3% of the vibration at point A; at point C, the vibration is about 90.9% of the vibration at point A; at point D, the vibration is about 87.5% of the vibration at point A. With the structure depth, the vibrations inside the geogrid reinforced embankment supported by CFG pile structure, are attenuated on average 1.2 times faster than the vibrations inside the conventional embankment structure.

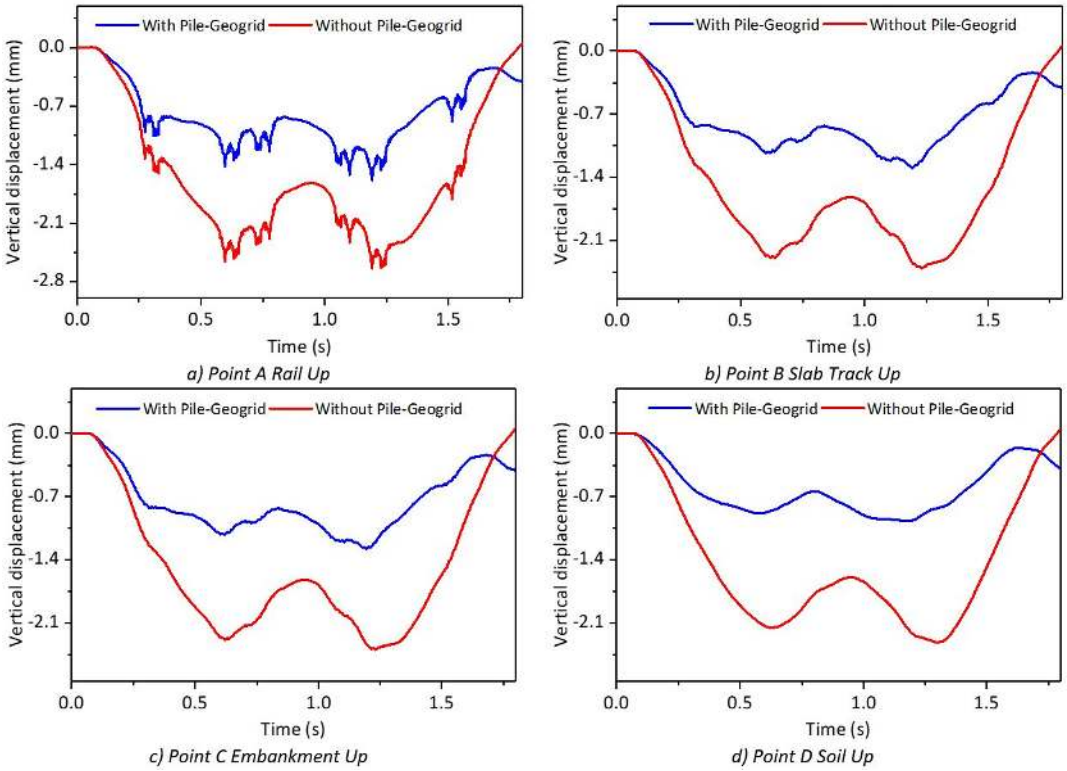

Figure 9: Time histories of the vertical displacement at the selected points

Table 6: Summary of the maximum displacement peak at the selected points

Section	Maximum Peak Displacement Structure conventional (mm)	Maximum Peak Displacement Structure reinforced (m)	Enhancement rate (%)
Rail Up	2.64	1.59	39.77
Track Slab Up	2.41	1.30	46.47
Embankment up	2.40	1.28	46.66
Soil up	2.31	0.97	58.01

In Figure 10, the vertical displacement as a function of depth is shown. It can be seen that the reinforced structure vertical displacement is less than the conventional embankment vertical displacement till 25.8 m of depth. The silty soil carrying the piles is localized at this depth and the sudden displacement increase in the structure reinforced can be explained by foundation layer behavior subjected to the dynamic train load absorbed by the piles. This observation is compatible with Thach work [22].

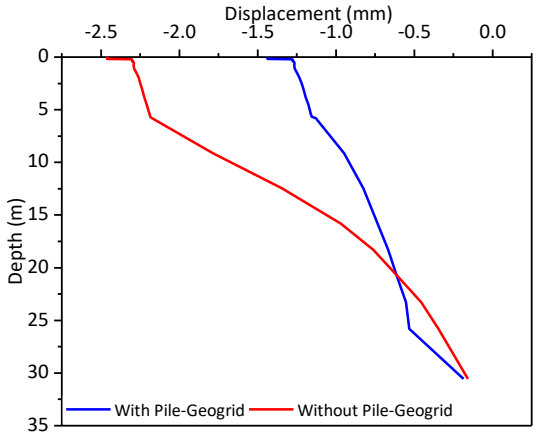

Figure 10: Displacement according to the depth right below the wheel

4.1.2 Vertical Velocity spectrum at soil up

The vertical velocity spectrum at the soil up (Point D) of the conventional embankment and the reinforced structure was computed by using the Fast Fourier transform and presented in Figure 11. It can be seen that the first peak of the amplitude apparent is larger and attenuates gradually. This can be explained by the quasi static state of the train weight when the first wheel is in contact with the selected point. Moreover. It is noticed that an amplitude peak is recorded after each frequency span of 2.2 Hz which corresponds to the passage of a carriage (25 m) running at 200 Km/h. The vertical velocity amplitudes for the conventional embankment are significantly larger than that for the reinforced embankment. The vibration amplitudes attenuate and tend to zero from 10.53 Hz and 24.39 Hz for reinforced embankment and conventional embankment respectively. The presence of piles in the soil enhances the capacity to respond to the vibration induced by train and attenuate quickly the vibration amplitude toward the soil.

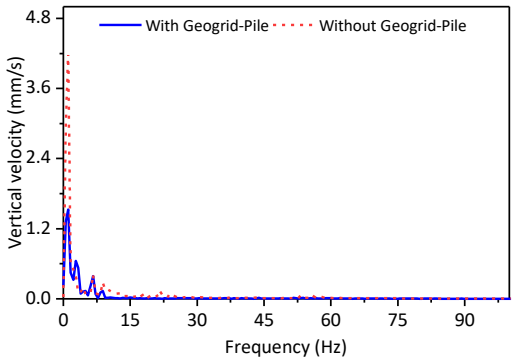

Figure 11: Vertical velocity spectrum at the soil up (Point D)

4.1.3 Magnitude of Displacement

Figure 12 shows the vibration propagation magnitude induced by a moving high speed train. It can be seen that in both cases the embankment is more affected by the vibration induced by the train. In the conventional embankment and the reinforced embankment, the magnitude of displacement observed in the embankment area below the train carriages varies from 2.21 mm to 1.412 mm and from 1.391 mm to 9.275 mm respectively. This large vibration magnitude observed in the conventional embankment is due to soil bearing weakness in which the vibration is almost as strong as the embankment. When the soil is improved by the pile and the embankment reinforced by geogrid, the attenuation of the vibration becomes more rapid and it is noticeable that the magnitude observed around the pile is small. This phenomenon is due to the rigidity conferred to the soil by pile and the stiffer platform effect of geogrid. Since strong dynamic amplification can be observed in the railway structures when the train approaches a certain speed depending on the properties of ground material [1, 22], this study shows that the pile and geogrid, because of their stiffness, provides the embankment with a certain rigidity to slacken the propagation of vibration induced by the train.

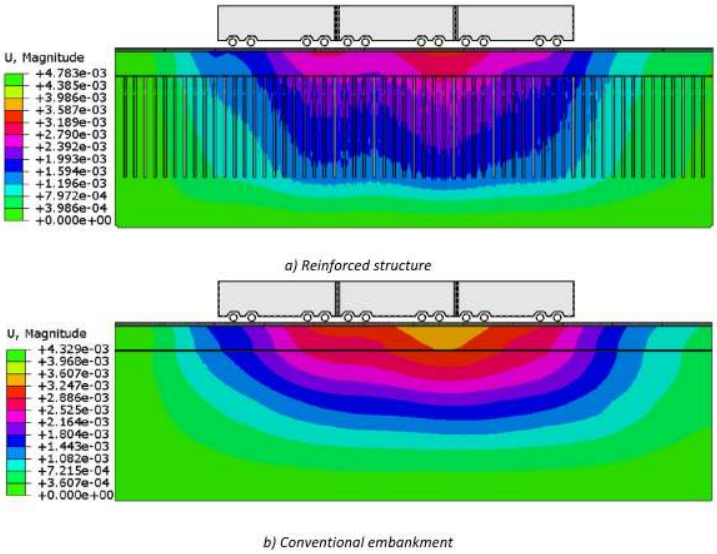

Figure 12: Cut view of the Magnitude of displacement (m)

4.1.4. Effect of train speed and overload

Several studies were carried out on the vibration of the railway embankment under train load moving and have shown that the increase in the train speed can increase the dynamic effect on the structure. When the train reaches a certain speed often called critical speed, the vibration induced by the train causes a large dynamic amplification in the whole structure. This phenomenon depends not only on the wave velocity of Rayleigh wave in an embankment-ground system but also on the minimum phase velocity of the bending wave propagating in the track [1, 4]. The track critical value depends on the physical properties of the ground media.

Figure 13a) shows the maximum vertical displacement of the rail track at point A according to the train speed. For the case of the conventional embankment structure, the maximum displacement is significantly high at all train speeds considered. The degree of dynamic amplification in the structure does not increase monotonically with increasing train speed but strongly depends on the existing relation between the natural vibration properties of the structure and the speed at which the train is moving. It is noticeable that the maximum displacement at 100 km/h, 260 km/h, and the speeds exceeding 400 km/h are particularly large and that a phenomenon of resonance is observed at the speed of 100 km/h and 260 km/h. This phenomenon has two primary causes. Firstly, since the structure is composed of various intrinsically dispersive materials, the wave field surface generated by the train load is mainly governed by two generalized modal waves whose propagation velocities characteristic are around 120 km/h. 200 km/h. When the train speed is close to these wave speeds, the dynamic response of the rail track is considerably amplified. This interpretation stems from the fabulous concept of critical speed. Thus, the train speeds at which dynamic amplification is strongly observed can be considered as the critical speeds of the structure. These critical velocities are governed by soil and embankment because of their low strength and therefore low wave velocities. This interpretation is also compatible with Thach work [30].

For the case of the geogrid-reinforced embankment supported by the CFG pile structure, the maximum displacement is reduced at all train speeds compared to the case of the conventional embankment structure. In particular, the phenomenon of resonance observed at the speed of 100 and 260 km/h is completely excluded, resulting in a reduction of 50% and 70% of the maximum displacement respectively. Moreover, when the high-speed train is moving at less than 150 km/h, the response is essentially quasi-static. This means that the inertial effect of the train, associated with speeds of less than. 150 km/h, contributes very little to the dynamic response of the geogrid reinforced embankment supported by CFG pile structure. These observations can be justified by the enhancement of soil and embankment cushion crushed stone layer by the inclusion of CFG piles and geogrid, which has led to an increase in their strength. These enhancements have resulted in a change in the natural vibration properties of the embankment and the soil. Thus, the dynamic response of the structure has changed accordingly and the phenomenon of resonance observed at a certain train speed has been annihilated.

During a train trip, it may happen that overload problems are encountered. The behavior of the railroad built over weak soil under different loads was investigated. Figure 13b} shows the vertical displacement variation of point A at the rail top with train wheel load when the load is 70, 120, 170 and 220 kN respectively. The maximum vertical displacement of point A during train carriages passage are compared. Regardless of the conventional or reinforced embankment, the vertical displacement increases gradually as the wheel load increases. The higher the wheel load, the greater the difference in vertical displacement caused by the same wheel load increases, indicating that the overload will deform the rail area. In addition, the vertical displacement of the geogrid reinforced embankment supported by CFG pile railway is smaller than that of conventional embankment under the same wheel load. With the augmentation of the wheel load, the difference between both displacements becomes more pronounced. When the wheel load is 220 kN, the maximum vertical displacement of the reinforced embankment and the conventional embankment are 5 mm and 10.5 mm respectively; the displacement reduction is 52.38%. it is shown that the geogrid reinforced embankment supported by CFG pile has an immense obvious effect on reducing the railway displacement caused by the overweight.

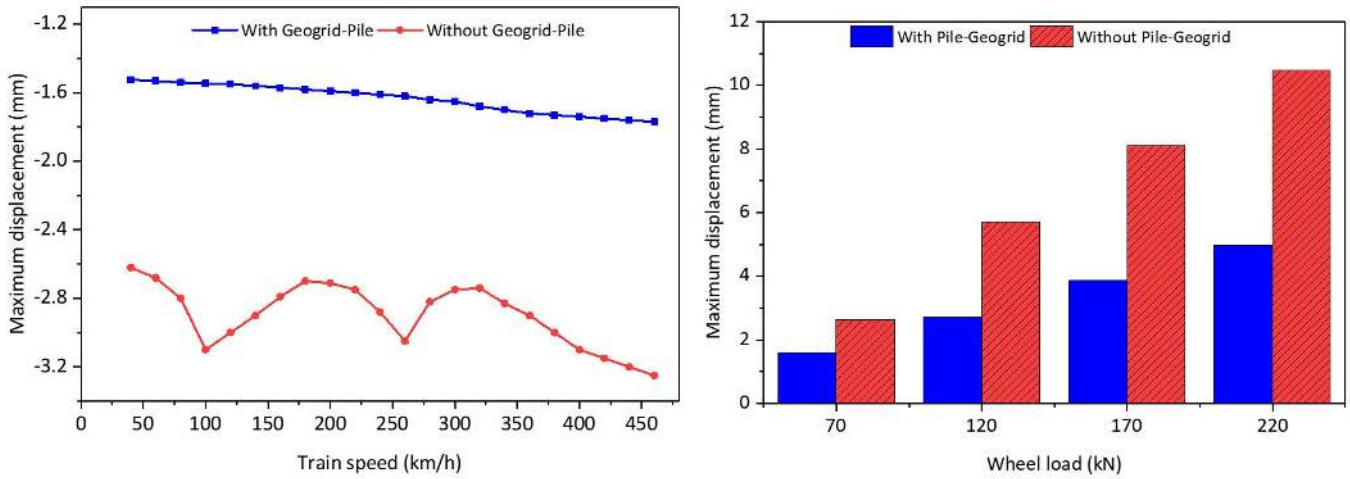

a) Peak vertical displacement at the rail top under train speed effect

b) Peak vertical displacement at the rail top under load effect

Figure 13: Peak vertical displacement at the rail top under train speed effect and overload

4.2 Distribution of Dynamic Stress

The stress distribution in the structure was investigated by analyzing the stress distribution in the embankment, the pile-soil stress and the stress developed in the geogrid.

4.2.1 Stress Distribution in the Embankment

Figure 14a) shows the stress in the structure according to the embankment depth. The Figure 14b) indicates the typical points of $P_{1\text{-}8}$ and $S_{1\text{-}8}$ located above the pile and the soil between piles.

The amplitude of stress increases gradually with the depth from P_1 to P_8, with 5.586×10^3 Pa at P_1, 5.740 kPa at P_2 from P_1 down to 0.4 m, 6.092 kPa at P_3 from P_1 down to 1.4 m, 6.270 kPa at P_4 from P_1 down to 2.7 m, 6.575 kPa at P_5 from P_1 down to 4.5 m, 7.510 kPa at P_6 from P_1 down to 4.65 m, 10.247 kPa at P_7 from P_1 down to 4.85 m and 30.934 kPa at P_8 from P_1 down to 5 m at the pile top. Conversely, the amplitude stress decreases gradually with depth from S_1 to S_8, with 19.310 kPa at S_1, 13.588 kPa at S_2 from S_1 down to 0.4 m, 8.575 kPa at S_3 from S_1 down to 1.4 m, 6.278 kPa at S_4 from S_1 down to 2.7 m, 5.237 kPa at S_5 from S_1 down to 4.5 m, 4.709 kPa at S_6 from S_1 down to 4.65 m, 4.318 kPa at S_7 from S_1 down to 4.85 m and 1.829 kPa at S_8 from S_1 down to 5 m at the soil top between piles.

At the embankment top, the stress at S_1 is quite close to that at P_1. The dynamic load of the train propagates in the same way in the embankment to a certain depth. At the soil level, the stress computed at P_8 is significantly larger than that at S_8. The dynamic stress in this numerical model is greater than that of the Xiao field test from which they reported that the dynamic stress at the top of the pile is 2.26 kPa and that on the ground between two adjacent piles is 1.96 kPa [31]. These recorded values are mainly due to the lightweight of the wheels of the train and the slow speed of the train adopted during their tests. Dynamic stress increases with the wheel weight and the train speed, as demonstrated by Jiang [32]. In addition, the embankment properties and its height also affect the distribution of dynamic stress. Thus, the stress computed above the pile in this study is different from that of xiao. Another reason is also the location of the typical points.

The ratio stress above the pile to that above the soil between piles at the same level is expressed as nj,

$$n_j = \frac{\sigma_{pj}}{\sigma_{sj}} \tag{7}$$

Where j is from 1 to 8; and σ_{pj} and σ_{sj} are the stress at the typical locations above the pile and soil respectively.

Table 7: Stress ratio n_j

j	1	2	3	4	5	6	7	8
n_j	0.28	0.42	0.71	0.9987	1.25	1.59	2.38	16.92

The stress concentration ratio in this study is n_8=16.92. The stress ratio shown in Table 7 gradually increases. This means that the dynamic train load transferred to the pile increase gradually with the embankment depth. The stress ratio n_6 shows the presence of a dynamic arching in the embankment. It was assumed that the point where the stress above the CFG pile is equal to that above the soil between piles is the arch. Thus, the vault height in the geogrid reinforced embankment supported by CFG pile structure under dynamic train loading is 2 m above the ground.

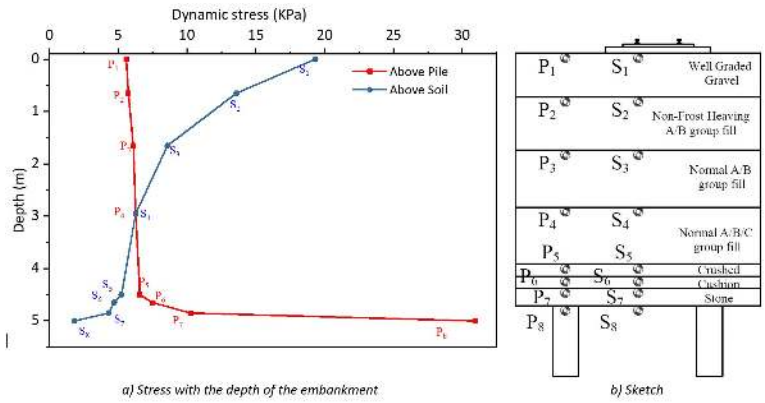

Figure 14: Stress along the embankment according to the depth

4.2.2 Pile-Soil Stress and Stress developed in Geogrid

The dynamic effect induced by train load in the time domain has been investigated at the pile top and the soil between piles top. The results are depicted in Figure 15a). It can be seen that the stress at the pile top is drastically larger at any time during the train operation. This clearly explains that the transfer load mechanism, in which a large part of dynamic train load (that should have been carried on the soil between the piles), is gradually absorbed by the pile and transferred to the bearing soil. This phenomenon is due to the rigidity difference between soil and CFG pile and the rigid platform effect provided by geogrid. This further reflects the advantages of the geogrid reinforced embankment supported by CFG pile structure in terms of bearing capacity relative to conventional embankments.

Furthermore, Figure 15b) shows the tensile stress developed in the low geogrid around three piles (Pile A, Pile B, and Pile C) located below the rail. It should be noted that the diameter of each pile was 0.5 m and that the spacing of the piles was 1.5 m center to center. As can be seen, the maximum computed tensile stress developed in the geogrid is about $17x10^3$ Pa and occurred at the pile edges. A large shape reduction of the tensile stress is observed from the pile edge toward the soil center and another small shape reduction is observed from the pile edge to the pile center. This observation can be explained as follows. Because the geogrid is placed above a layer of clay reinforced by the piles, the ground will be more resistant in the zone of the piles. Thereby, the geogrid, which is a flexible fiber assembly, will necessarily bear on the most rigid zone to resist the deformation caused by the pressure to which it is subjected. Consequently, the geogrid is more stretched at the edge of the piles and thus transfer a part of the pressure exerted on it. This justifies the role of a rigid platform of the geogrid in the embankment.

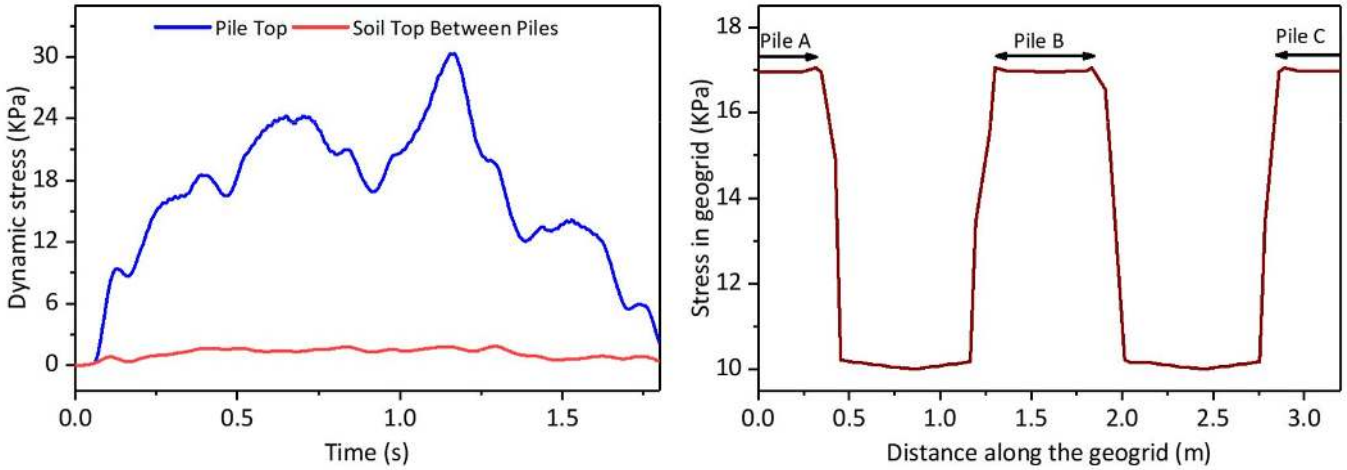

a) Time histories of the dynamic pressure at point D (Soil between piles) and point E (Pile Up)

b) The stress developed in geogrid

Figure 15: Time histories of the pile-soil stress and the stress developed in geogrid

4.3 Effect of Geogrid Tensile Strength and Pile Strength Grade

The influence of geogrid tensile strength on the structure vibration during the train operation was evaluated. For this purpose, three cases of biaxial geogrid with an ultimate tensile strength of 30 kN/m, 50 kN/m and 80 kN/m, were used in the numerical model and the results of the maximum displacement at the rail top are shown in Figure 16a). The displacement at any train speed decreases as the geogrid is strengthened. The maximum displacements and the gap between the displacements during the variation of the speed were summarized in Table 8 to get a better view and interpretation of the graph.

Table 8: Summary of the maximum displacement at the rail top according to geogrid tensile strength

Geogrid		Maximum displacement (mm) according to Speed			Gap between displacement during speed variation	
Designation	Ultimate tensile strength (kN/m)	100km/h	200km/h	300km/h	100km/h to 200km/h	200km/h to 300km/h
Geo 1	30	1.5563	1.5946	1.6595	0.0000383	0.0000649
Geo 2	50	1.5552	1.557	1.6483	0.0000305	0.0000626
Geo 3	80	1.5495	1.5728	1.6243	0.0000233	0.0000515

Referring to the results when the train is at 100 km / h, the displacements obtained while using Geo 1, Geo 2 and Geo 3 are 1.5563 mm, 1.5552 mm, and 1.5495 mm respectively. The decrease rate is 0.07% when Geo 1 is replaced by Geo 2 and 0.43% when Geo 1 is replaced by Geo 3. Moreover, during the variation of the speed of the train, the gap between the displacements is much smaller when the embankment is reinforced by Geo 3. The reduction of the vibration in the structure is scanty (regardless of the strength of geogrid used) but the utilization of a geogrid with high tensile strength is important in the regulation of the vibration in the structure during the train operation. The more resistant it is, the better it regulates.

In addition, the influence of pile strength grade on the structure vibration during the train operation is also evaluated. For this purpose, three cases of pile with strength grade (C25, C60, and C80) were used in the numerical model and the results of the maximum displacement at the rail top are shown in Figure 16b). The displacement at any train speed decreases as the pile is strengthened. The maximum displacements and the gap between the displacements during the variation of the train speed were summarized in Table 9 to get a better view and interpretation of the graph.

Table 9: Summary of the maximum displacement at the rail top according to pile strength grade

Pile strength grade	Maximum displacement (mm) according to Speed			Gap between displacement according to the speed	
	100km/h	200km/h	300km/h	100km/h to 200km/h	200km/h to 300km/h
C25	1.5528	1.5886	1.6679	0.0000358	0.0000793
C60	1.3301	1.3512	1.4042	0.0000211	0.000053
C80	1.3045	1.3167	1.3438	0.0000122	0.0000271

Referring to the results when the train is at 300 km/h, the displacements obtained while using C25, C60 and C80 are 1.6679 mm, 1.4042 mm, and 1.3438 mm respectively. The decrease rate is 15.81% when the grade C25 is replaced by the grade C70 and 19.43% when the grade C25 is replaced by the grade C80. Moreover, during the variation of the speed of the train, the gap between the displacements was much smaller when the soil is improved by the pile with strength grade C80. The reduction of the vibration in the structure is larger, regardless of the strength grade of pile used. Since it is known that the change of vibration in the structure during the operation of the train can affect the comfort of the passengers, it is preferable to use a high-strength pile to regulate the variation of the vibration in the structure, to tackle this problem.

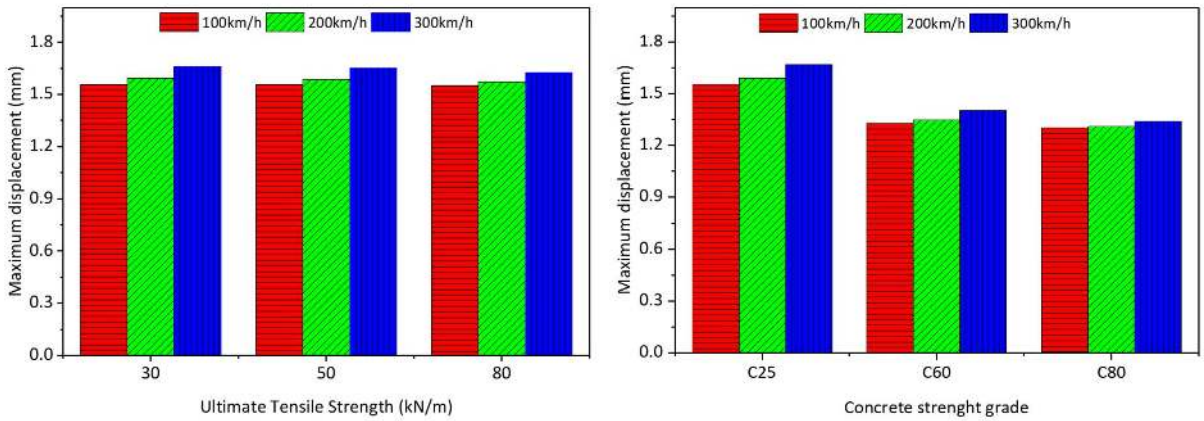

a) Peak vertical displacement at the rail top under geogrid tensile strength

b) Peak vertical displacement at the rail top with different pile strength grade

Figure 16: Peak vertical displacement at the rail top under geogrid tensile strength and pile strength grade

5 Conclusion

In this study, the dynamic response of an instrumented geogrid reinforced embankment supported by CFG pile test section was investigated. A three-dimensional non-linear finite element was established to accurately simulate the dynamic characteristic of the instrumented test section under different train speed, load condition and coupling effect of geogrid and pile with various strength. The train multiple wheels' load was incorporated in the model as a transient moving load through a developed Fortran subroutine (Dload). The numerical model reliability was verified by comparing the simulation results with the data obtained from field test carried out on the Harbin-Dalian railway section. The following conclusions were drawn:

- The dynamic stress and the accelerations computed by the established 3D FE model are consistent with that measured at Harbin-Dalian railroad section indicating that the developed model can be employed to predict the dynamic behavior of a rail track accurately.
- An evaluation of the role of the piles and geogrid on the dynamic response of the railway shows that their presence contributes to a large reduction of the displacement in the structure with a rate varying from 39% to 58% according to the rigidity of each material of the structure. The attenuation of the vibration along the structure in depth is on average 1.2 times faster. The geogrid reinforced embankment supported by CFG pile structure enhance the railroad system performance by minimizing the propagation of vibrations induced by the train passage.
- The piles improve the vibration properties of the soil and the geogrid improves that of the embankment. This allows an elimination of the large dynamic amplifications observed in the structure when the speed of the train approaches respectively 100 km / h and 260 km / h. In addition, the response of the geogrid reinforced embankment supported by CFG pile structure is almost static for speeds less than 150 km / h. Apart from this, the rigidity conferred by the piles and geogrids on the ground and the embankment also has an immense influence on the reduction of the vibration caused by the overloads.
- The analysis of the stress distribution in the structure indicates that, depending on the variation of the stresses above the soil and the pile, an arching is formed in the embankment about 2 m above the ground. a large part of the dynamic load of the train is exerted on the piles. The stress developed in the geogrid is significantly larger at the edge of the CFG pile below. This phenomenon leads to the transmission of some of the pressure exerted on the geogrid towards the top of the pile. Thus, much of the dynamic load induced by the train is absorbed by the CFG piles and transferred to the carrier ground.
- The variation of the speed of the train makes that the structure is subjected to a non-constant vibration, thus affecting the comfort of the passengers. The coupling effect of a geogrid with different tensile strengths and a pile with different grades indicates that the combination of a high strength pile and a geogrid significantly reduces the displacement gap due to the variation speed of the train. Thereby, the vibrations observed during the train operation, are almost constant and the passengers' comfort is guaranteed. The dynamic response of geogrid-reinforced embankment supported by CFG pile deserves further investigation to eliminate any significant vibration that may be critical to transportation safety. A good design of railroad over weak soil will reduce tremendously, if not totally eliminate the discomfort passengers experience.

Acknowledgements

This work was supported by the State Key Program of National Natural Science Foundation of China (Grant No.41430634, 41627801 and U1834206), and the Technology Research and Development Plan Program of China Railway Corporation (Grant No. 2016G002-F).

Author's Contributions: Conceptualization, IVL Chango; Data curation, IVL Chango and OC Assobga; Formal analysis, OC Assobga and IVL Chango; Funding acquisition, M Yan, X Ling and L Tang; Investigation, M Yan, X Ling, L Tang and IVL Chango; Methodology, IVL Chango; Project administration, X Ling and L Tang; Resources, X Ling and L Tang; Software, IVL Chango and OC Assobga; Supervision, X Ling, L Tang and M Yan; Validation, IVL Chango, OC Assobga and M Yan; Visualization, IVL Chango, Writing – original draft, IVL Chango; Writing – review & editing, IVL Chango, OC Assobga, M Yan, X Ling, and L Tang.

Editor: Marcílio Alves.

Reference

1. Madshus, C.c. and Kaynia, A." High-speed railway lines on soft ground: dynamic behaviour at critical train speed". Journal of Sound and Vibration, 2000. 231(3): p. 689-701. DOI: 10.1006/jsvi.1999.2647.

2. Hu, J., Bian, X. and Jiang, J. "Critical velocity of high-speed train running on soft soil and induced dynamic soil response". Procedia engineering, 2016. 143: p. 1034-1042. DOI: 10.1016/j.proeng.2016.06.102.

3. Kaynia, A.M., Madshus, C. and Zackrisson, P. “Ground vibration from high-speed trains: prediction and countermeasure”. Journal of Geotechnical and Geoenvironmental Engineering, 2000. 126(6): p. 531-537. DOI: 10.1061/(ASCE)1090-0241(2000)126:6(531).

4. Krylov, V.V., Dawson, A., Heelis, M., and Collop, A., “Rail movement and ground waves caused by high-speed trains approaching track-soil critical velocities”. Proceedings of the Institution of Mechanical Engineers, Part F: Journal of Rail and Rapid Transit, 2000. 214(2): p. 107-116. DOI: 10.1243/0954409001531379.

5. Raithel, M., Kirchner, and Kempfert, H. “German recommendations for reinforced embankments on pile-similar elements”, in Geosynthetics in Civil and Environmental Engineering. 2008, Springer. p. 697-702. DOI: 10.1007/978-3-540-69313-0_128.

6. Cheng, Q., Wu, J., Zhang, D., and Ma, F., “Field testing of geosynthetic-reinforced and column-supported earth platforms constructed on soft soil”. Frontiers of Structural and Civil Engineering, 2014. 8(2): p. 124-139. DOI: 10.1007/s11709-014-0255-9.

7. Liu, H., Ng, C.W. and Fei, K. “Performance of a geogrid-reinforced and pile-supported highway embankment over soft clay: case study”. Journal of Geotechnical and Geoenvironmental Engineering, 2007. 133(12): p. 1483-1493. DOI: 10.1061/(ASCE)1090-0241(2007)133:12(1483).

8. Wu, L., Jiang, G., Liu, X., Xiao, H., and Sheng, D., “Performance of geogrid-reinforced pile-supported embankments over decomposed granite soil”. Proceedings of the Institution of Civil Engineers-Geotechnical Engineering, 2017. 171(1): p. 37-51. DOI: 10.1680/jgeen.17.00009.

9. Ariyarathne, P. and Liyanapathirana, D. “Review of existing design methods for geosynthetic-reinforced pile-supported embankments”. Soils and Foundations, 2015. 55(1): p. 17-34. DOI: 10.1016/j.sandf.2014.12.002

10. Zhang, C., Jiang, G, Liu, X, and buzzi, o., “Arching in geogrid-reinforced pile-supported embankments over silty clay of medium compressibility: Field data and analytical solution”. Computers and Geotechnics, 2016. 77: p. 11-25. DOI: 10.1016/j.compgeo.2016.03.007.

11. Briançon, L. and. Simon, B., “Performance of pile-supported embankment over soft soil: full-scale experiment”. Journal of Geotechnical and Geoenvironmental Engineering, 2011. 138(4): p. 551-561. DOI: 10.1061/(ASCE)GT.1943-5606.0000561.

12. Lai, H.-J., -J., Zheng, J.-J., Zhang, J., Zhang, R.-J., and Cui, L., “DEM analysis of “soil”-arching within geogrid-reinforced and unreinforced pile-supported embankments”. Computers and Geotechnics, 2014. 61: p. 13-23. DOI: 10.1016/j.compgeo.2014.04.007.

13. Heydari-Noghabi, H., Varandas, J., Esmaeili, M., and Zakeri, J., “Investigating the influence of auxiliary rails on dynamic behavior of railway transition zone by a 3D train-track interaction model”. Latin American Journal of Solids and Structures, 2017. 14(11): p. 2000-2018. DOI: 10.1590/1679-78253906.

14. Real, J., Zamorano, C., Asensio, T., and Montalbán., “Comparison of the effect of different sleeper typologies and track layout on railway vibrations”. Latin American Journal of Solids and Structures, 2014. 11(12): p. 2241-2254. DOI: 10.1590/S1679-78252014001200007.

15. Sol-Sánchez, M., Moreno-Navarro, F. and Rubio-Gámez, M.C. “An analysis of the performance of deconstructed tires for use as pads in railroad tracks”. Journal of Civil Engineering and Management, 2016. 22(6): p. 739-746. DOI: 10.3846/13923730.2014.914098.

16. Hua, L., Fujun, N., Yonghong, N., and Xifeng, Y., “Study on thermal regime of roadbed–culvert transition section along a high speed railway in seasonally frozen regions”. Cold Regions Science and Technology, 2014. 106: p. 216-231. DOI: 10.1016/j.coldregions.2014.07.008.

17. Sun, Q., Zhang, X., Yang, Y., and Liu, J, “Research on settlement of pile-net composite foundation of high-speed railway in soft soil area”. Guangxi Daxue Xuebao(Ziran Kexue Ban), 2013. 38(1): p. 157-164.

18. Yang, J., Kong, B., Cai, C., and Wang, J. S., “Behavior of High-Speed Railway Ballastless Track Slabs Using Reactive Powder Concrete Materials”. Journal of Transportation Engineering, 2016. 142(8): p. 04016031. DOI: 10.1061/(ASCE)TE.1943-5436.0000849.

19. Chen, J. and Zhou, Y. “Dynamic responses of subgrade under double-line high-speed railway”. Soil Dynamics and Earthquake Engineering, 2018. 110: p. 1-12. DOI: 10.1016/j.soildyn.2018.03.028.

20. Yin, F., Zhou, H., Liu, H., & Chu, J., “Experimental and numerical analysis of XCC pile-geogrid foundation for existing expressway under traffic load”. International Journal of Civil Engineering, 2018. 16(10): p. 1371-1388. DOI: 10.1007/s40999-017-0267-7.

21. Gao, G., Chen, J., Song, J., Yang, J., and Yao, S. “Field measurement and analysis of ground vibration induced by high-speed train”. in International Symposium on Environmental Vibration and Transportation Geodynamics. 2016. Springer. DOI: 10.1007/978-981-10-4508-0_11.

22. Thach, P.-N., Liu, H.-L. and Kong, G.-Q. “Vibration analysis of pile-supported embankments under high-speed train passage”. Soil Dynamics and Earthquake Engineering, 2013. 55: p. 92-99. DOI: 10.1016/j.soildyn.2013.09.006.

23. Zienkiewicz, O.C., Taylor, R. L., Nithiarasu, P., and Zhu, J., The finite element method. Vol. 3. 1977: McGraw-hill London.

24. Lysmer, J. and R.L. Kuhlemeyer, Finite dynamic model for infinite media. Journal of the Engineering Mechanics Division, 1969. 95(4): p. 859-878.

25. Kouroussis, G., Verlinden, O. and Conti, C. “Finite-dynamic model for infinite media: corrected solution of viscous boundary efficiency”. Journal of Engineering Mechanics, 2011. 137(7): p. 509-511. DOI: 10.1061/(ASCE)EM.1943-7889.0000250.

26. Bathe, K.-J., Finite element procedures. 2006: Klaus-Jurgen Bathe.

27. Nåvik, P.R., “Numerical Analysis of the Dynamic Behaviour of Railway Catenary Systems in Accordance with Norwegian Conditions”. 2013, Institutt for konstruksjonsteknikk.

28. Assogba, O.C., Tan, Y., Sun, Z., Lushinga, N. and Bin, Z., “Effect of vehicle speed and overload on dynamic response of semi-rigid base asphalt” pavement. Road Materials and Pavement Design, 2019: p. 1-31.

29. Bian, X., Jiang, H., Chang, C., Hu, J., and Chen, Y., “Track and ground vibrations generated by high-speed train running on ballastless railway with excitation of vertical track irregularities”. Soil Dynamics and Earthquake Engineering, 2015. 76: p. 29-43. DOI: 10.1016/j.soildyn.2015.02.009.

30. Thach, P.-N., Liu, H.-L. and Kong, G.-Q. “Evaluation of PCC pile method in mitigating embankment vibrations from a high-speed train”. Journal of Geotechnical and Geoenvironmental Engineering, 2013. 139(12): p. 2225-2228. DOI: 10.1061/(ASCE)GT.1943-5606.0000941.

31. XIAO, H., JIANG, G.-l. and WEI, Y.-x. “Dynamic Test Analysis on Ballastless-track Column-net Structure Subgrade of the Suining-Chongqing Railway Line” [J]. Journal of the China Railway Society, 2010. 1.

32. Jiang, H., Bian, X., Xu, X., Chen, Y., and Jiang, J.,” Full-scale model tests on dynamic performances of ballastless high-speed railways under moving train loads”. Chinese Journal of Geotechnical Engineering, 2014. 36(2): p. 354-362.